Intermetallics 19 (2011) 577–585

Contents lists available at ScienceDirect

Intermetallics

journal homepage: www.elsevier.com/locate/intermet

Cyclic pseudoelastic behavior and energy dissipation in as-cast Cu-Zn-Al foams of different densities

G. Bertolino [a,b,*], A. Gruttadauria [c], P. Arneodo Larochette [a,b], E.M. Castrodeza [d], A. Baruj [a,b], H.E. Troiani [a,b]

[a] Centro Atómico Bariloche and Instituto Balseiro, CNEA, 8400 S.C. Bariloche, Argentina
[b] CONICET, Argentina
[c] Dipartimento di Meccanica, Politecnico di Milano, Via G. La Masa 34, 20156 Milan, Italy
[d] Department of Metallurgical and Materials Engineering, COPPE-UFRJ, Rio de Janeiro, CP 68505, 21941-972 Rio de Janeiro, Brazil

ARTICLE INFO

Article history:
Received 10 September 2010
Received in revised form
4 November 2010
Accepted 8 December 2010
Available online 31 December 2010

Keywords:
B. Shape memory effects
D. Martensitic structure
F. Mechanical testing
G. Shape memory alloy applications

ABSTRACT

This paper presents a study of the mechanical properties of pseudoelastic Cu-Zn-Al foams. Foams of different densities were cycled in compression. The paper shows the retained/dissipated energy by the material, i.e. the area of the compression cycle, as a function of the material density. The frequency and strain amplitude, usual parameters that may influence the damping properties, are studied by evaluating the dissipated energy and the specific damping capacity. Samples cyclically tested under constrained compression conditions show a remarkable mechanical stability and reproducibility. The material does not appreciably degrade after 1000 compression cycles at room temperature. We emphasize the material does not need any thermomechanical processing or training treatment in order to present the mechanical properties detailed in the present paper.

1. Introduction

The development of metallic shape memory foams (SMFs) has attracted considerable attention during the last years. The main goal has been finding a material that combines the shape recovery properties associated to martensitic pseudoelasticity with the typical features of cellular metals [1–3]. Most of the efforts have been directed to the synthesis and characterization of SMFs based on the Ni-Ti system [4] due to the fact that Ni-Ti shape memory alloys (SMAs) have excellent shape memory properties [5]. However, in order to attain those high recovery properties in Ni-Ti, it is necessary to perform suitable thermomechanical treatments. The goal is to reduce the grain size and to harden the B2 austenite. The latter can be achieved either by introducing plastic deformation or by producing a fine distribution of Ti_3Ni_4 precipitates in Ni-rich alloys [5]. Many of the mechanical treatments useful for improving dense Ni-Ti SMAs are not applicable in the case of Ni-Ti foams due to the nature of the materials themselves. For example, performing rolling, drawing or swaging would destroy the foam morphology. As a consequence, the possibilities of obtaining pseudoelastic Ni-Ti foams are quite limited. The explored paths usually involve sintering of extremely refined pre-alloyed Ni-Ti powders and, in some cases, producing a dispersion of Ti_3Ni_4 precipitates by applying a thermal treatment at high-temperature [4,6–10]. Both possibilities present some drawbacks. In the former, it is necessary to process the potentially pyrophoric powder under inert atmosphere or vacuum and to control the sintering temperature very precisely because sintered particles tend to agglomerate and grow into larger undeformed grains with the subsequent loss of shape memory properties, and to form undesired intermetallic phases like Ni_3Ti [6–9]. The latter involves performing heat treatments at intermediate temperatures (usually at around 550 °C) in order to precipitate the Ti_3Ni_4 phase while protecting the foam surface from oxidation [6,9]. Although promising results have been achieved [10], the associated costs involved in these procedures add to the already high costs of raw materials and alloy processing. Alternative processing methods, such as the extensively researched self-propagating high-temperature synthesis (SHS), result in brittle foams able to recover pseudoelastically only a fraction of the stress-induced deformation [4,11]. The main problems related to this method are the formation of undesirable phases [11–13], presence of excess unalloyed Ni [12] and partial melting of the material during the synthesis [13]. Better results were obtained by carefully controlling the temperature during the synthesis of elemental powders [14,15]. However, the pseudoelastic behavior of Ni-Ti foams tends to deteriorate under cyclic loads [16] and the foams

* Corresponding author.
E-mail address: bertolin@cab.cnea.gov.ar (G. Bertolino).

0966-9795/$ – see front matter © 2010 Elsevier Ltd. All rights reserved.
doi:10.1016/j.intermet.2010.12.008

have inferior corrosion properties as compared to the dense material [17]. For these reasons, the development of Ni-Ti foams currently focuses on the production of medical devices where the biocompatibility of the material is an important advantage and high costs can be circumvented in order to obtain a desired application [4,8,18]. On the same grounds, their use in structural applications, where massive quantities are necessary and cost constitutes an important factor, is ruled out. Therefore, there are open opportunities for the development of alternative SMFs based on different alloys. Indeed, several studies aimed at finding suitable alloy candidates for producing structural SMFs are reported in the literature. The most promising involve the use of Fe-based [19] and Cu-based SMAs [20,21]. Among them, Cu-Zn-Al SMAs are of particular interest.

Martensitic transformations in the Cu-Zn-Al system have been studied for a long time in relation to their very good associated shape memory properties [22]. Depending on the chemical composition, Cu-Zn-Al alloys can have a cubic austenitic (often referred as β phase) or a compact martensitic structure at room temperature. On its side, the β phase displays a B2 (CsCl) or a $L2_1$ order depending on the elements concentration [22]. Each of them transforms to a different martensite on cooling or when applying mechanical stress. While the B2 ordered phase transforms to a 9R martensite, the β phase with $L2_1$ order transforms to 18R martensite. Both martensites inherit a certain order from β and evolve to more stable ordered structures even at room temperature in a process known as stabilization [22]. In general, the pseudoelastic properties of dense polycrystalline Ni-Ti martensitic alloys are better than the analogous properties for the Cu-Zn-Al system. However, considering foam production Cu-Zn-Al SMAs have some important practical advantages. The alloys can be prepared by simple standard melting techniques showing good pseudoelastic properties already in the as-quenched condition [22]. The alloys melting temperatures are lower than in the case of Ni-Ti, allowing for different foaming procedures like, for example, liquid phase processing. Recently, a method useful to synthesize Cu-Zn-Al SMFs has been reported [21,23]. It consists of the infiltration of molten metal into a bed of silica particles, which are then leached through a suitable chemical attack. The method enables to obtain foams of different densities, pore morphology and mean pore size. The obtained foams reported by Castrodeza et al. [21] need a thermal treatment due to the fact that the as-cast foam contains a mixture of α and β-phases. On the contrary, the foams reported by Bertolino et al. [24] present only a β-phase in the as-cast condition and display good pseudoelastic properties without the need of performing special thermomechanical treatments [24].

The recent development of Cu-Zn-Al SMFs opened several questions regarding their mechanical behavior and structural stability. First, up to the authors' knowledge, the variation of mechanical parameters such as the transformation stress and absorbed mechanical energy with the foam density has never been reported for this new material. Second, it is still not clear whether the foams can stand cyclic loads or not. Cu-Zn-Al SMFs were shown to develop intergranular fracture at moderated strain levels [24]. It is then critical to study the possibility of performing repeated loading/unloading pseudoelastic cycles because that would be the one of the main functionalities sought for these materials. Third, the influence of frequency and vibration amplitude on the damping characteristic of the foam is important to be evaluated. The use of this type of material in practical applications will depend on the frequency and vibration amplitude ranges in which the damping capacity is elevated. The stability of damping under operating conditions will be also a factor affecting the applicability of these materials.

Table 1
Main characteristics of the Cu-Zn-Al foams under study.

Specimen	Pore size [mm] Mean [min–max]	Density [kg/m^3]	Relative density	Diameter [mm]	Height [mm]
a	4.1 [3.4–4.6]	1870	0.22	24	28.0
b	2.9 [2.1–3.3]	2300	0.27	21	26.8
c	2.1 [1.6–2.5]	2350	0.28	23	24.0
d	2.9 [2.1–3.3]	2160	0.25	21	23.0
e	2.1 [1.6–2.5]	3150	0.40	21	26.0
f	2.1 [1.6–2.5]	2434	0.30	22	22.0

2. Experiments

Experiments were performed on foams with a composition of Cu-16.1Zn-7.9Al (wt. %), corresponding to a martensite start temperature Ms = 10 °C and an electron concentration e/a = 1.48. For this composition, the room temperature phase in the unloaded condition is β with a $L2_1$ crystallographic ordered structure. The material will then transform to the 18R martensite upon loading or on cooling [22]. A standard pure Cu foam was also prepared in order to perform comparisons with the pseudoelastic material.

In order to produce the foams, pure metals were alloyed in Vycor capsules under Ar atmosphere in a vertical resistive furnace. The resulting alloy specimens weighted around 80 g. By using these alloys as starting materials, foams were obtained by the method described in detail in Ref. [21,23]. Briefly, the alloys were re-melted in an open induction furnace using pure carbon crucibles. After melting them, the temperature was kept at about 100 °C above the melting point and dried silica gel (SiO_2) spherical particles were pressed into the liquid. Details on the particle sizes used for this work are provided in Table 1. The mixtures of alloys and particles were left to solidify inside the crucibles. Afterwards, the SiO_2 particles were leached in an HF aqueous solution that does not affect the metallic matrix. As a consequence, cylinders of polycrystalline Cu-Zn-Al foams in the β phase were obtained.

We observed the samples by using a Philips 505 scanning electron microscope (SEM) with a tungsten filament operating at 20 kV. The resulting material presented an open-cell structure and relative densities with respect to the bulk alloy (from this point on referred simply as "relative densities") in the range of 0.2–0.4. The foam densities were measured directly by calculating the ratios between the weight and the volume. Pictures showing images of foams with different pore sizes are presented in Fig. 1, microstructural features of these foams are indicated in Table 1. The microstructure of the foam materials was observed by using an optical microscope and images were obtained with a digital camera. The foam consists on struts limiting the spheroidal voids left by the etched SiO_2 particles (Fig. 2). The material constituting the struts is polycrystalline. The grain boundaries can be observed in Fig. 2. In this case, the grains are big enough to occupy the complete width of the struts. For this reason, the grain size is in part limited by the shape of struts.

Cylindrical compression specimens were carefully machined from the main porous material in order to eliminate the effect of the irregular external layer. The dimensions of the compression samples (diameter φ from 21 mm to 24 mm and length l from 23 mm to 28 mm) were adjusted according to the pore size in order to have at least 7–8 pores in every direction. Quasi-static compression tests were performed by using an Instron 1123 mechanical testing machine at room temperature (22 °C) under displacement control at a crosshead speed of 0.1 mm/min. Cyclic compression test were performed by using an MTS 810 servo-hydraulic machine imposing a sinusoidal deformation wave also at room temperature (22 °C). The control parameters of cyclic test

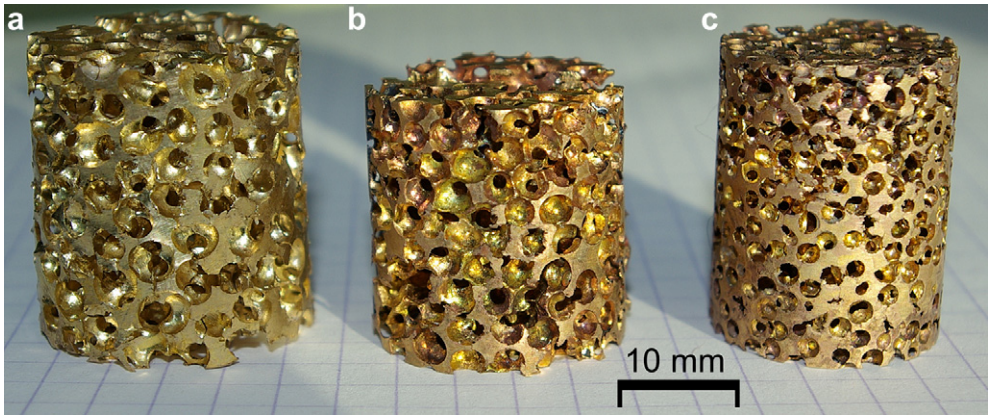

Fig. 1. Images corresponding to Cu-Zn-Al foams of different mean pore size. (a) 4 mm, (b) 3 mm and (c) 2 mm. The scale bar is depicted in the figure.

were the frequency of excitation and the maximum peak to peak strain amplitude. Surface friction was reduced by slightly covering the foams surface with silicon grease. The strain was measured with an extensometer attached to the compression plates.

In this paper we report the mechanical response and transformation properties of the *as-cast* Cu-Zn-Al foams. Apart from the foaming procedure, the fabrication steps do not involve thermo-mechanical treatments of any kind.

3. Results and discussion

3.1. Stress-strain response

Fig. 3 shows the stress-strain curves obtained for a Cu-Zn-Al pseudoelastic foam (a) and an elasto-plastic Cu foam (b). Both foams have been manufactured with the same space holder size, thus resulting in similar microstructural characteristics. The nominal stress has been calculated by using the foam samples complete face area. The curves show two very different responses.

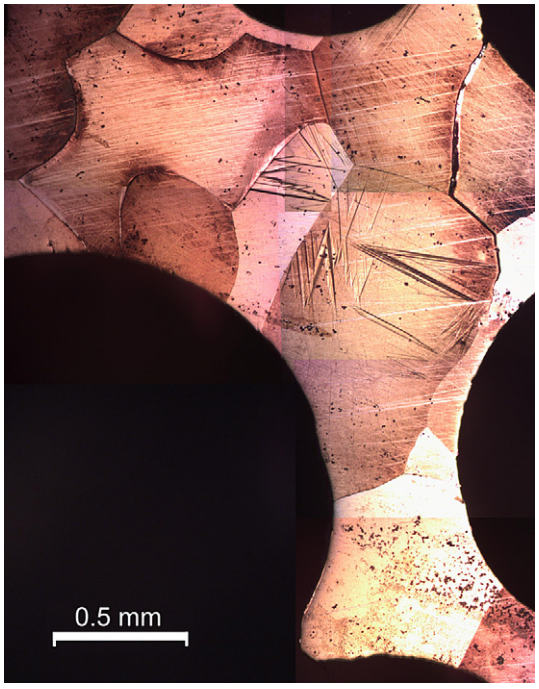

Fig. 2. Image obtained with the optical microscope showing the polycrystalline nature of the Cu-Zn-Al foams. The scale bar is shown in the image.

When load is applied to a pseudoelastic foam, Fig. 3a, the stress-strain curve starts to grow linearly as expected for the linear elastic deformation regime where cell edge bending occurs [25]. Afterwards, a change in the slope (point σ_T in the figure) marks the threshold where the martensitic transformation in the materials starts. The new slope shows also a quasi-linear behavior where the martensitic transformation governs the deformation process. After attaining a specific strain level, the external force was gradually reduced and the sample spontaneously recovered a significant amount of the achieved strain. There is a mechanical hysteresis because the direct and reverse martensitic transformations occur at different stress levels. The permanent plastic deformation usually suffered by non-transforming metallic foams under the action of an external stress is replaced in this new type of materials by a phase transformation and the material is able to almost recover its original dimensions when the external stress vanishes. The area enclosed by the loading/unloading cycles is the specific energy retained and dissipated by the material during the transformation/retransformation process.

For comparison, the mechanical response of a pure Cu foam is shown in Fig. 3b, displaying the typical behavior of elasto-plastic cellular materials [25]. This curve shows a linear elastic region where strut bending occurs followed by a plateau corresponding to plastic yielding. The densification stage could be observed in the extended range figure presented as an inset. The curve also shows partial unloads. The unload curve in each case is linear and they are parallel to each other indicating the elasto-plastic characteristic of the material.

The results presented in Fig. 3 imply a martensitic behavior of the material. The shapes of stress-strain compression curves show all the typical features of a pseudoelastic curve for a Cu-Zn-Al polycrystal (see for example Ref. [24]).

In order to understand the behavior of the foams, we analized the response of a bulk material ($\rho/\rho_{bulk} = 1$) of the same composition and grain size by studying the temperature evolution of the critical stress. The critical stress is defined as the change in the slope of the stress-strain curve. We see that the deformation process presents two different regimes (Fig. 4). At low temperatures there is a linear increase for the critical stress as a function of temperature. The low temperature behavior can be explained by the Clapeyron equation [22], this being consistent with fact that the critical stress is associated with the formation of stress-induced martensite. Beyond a specific temperature threshold, the critical stress diminishes if the temperature increases even more. In this regime, the critical stress corresponds to the yield stress of the material. The linear extrapolation of the plastic deformation regime up to room temperature approximates the value of the austenite yield stress.

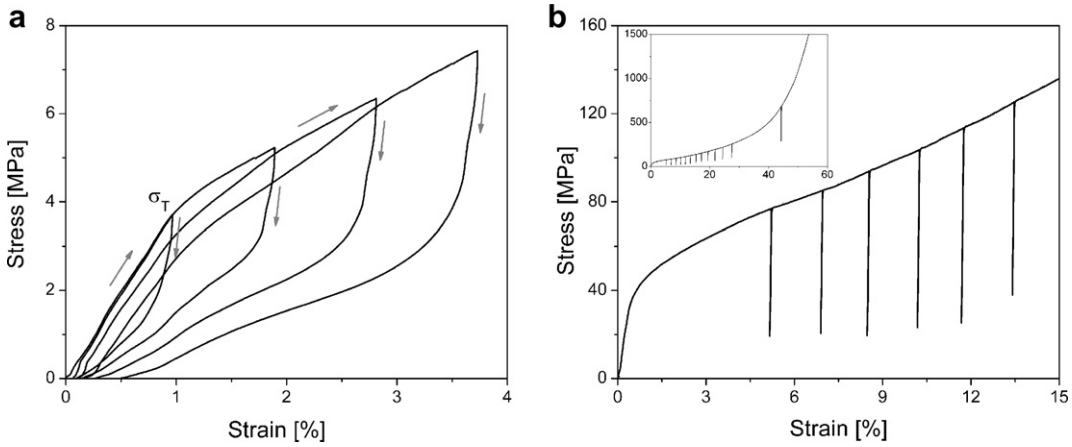

Fig. 3. (a) Stress-strain curves corresponding to compression tests performed at different final strain levels on a pseudoelastic Cu-Zn-Al foam. Critical point σ_T marks the onset of the stress-induced martensitic transformation. (b) Stress-strain compression curve corresponding to a pure Cu foam with similar density as the pseudoelastic sample presented in (a). The applied load has been decreased at regular intervals, resulting in parallel unloading lines. This is the typical behavior of a standard elasto-plastic metal foam. The inset in the figure presents an extended stress-strain range, showing the foam densification.

At room temperature, the approximate austenite yield stress (σ_Y = 860 MPa) is well above the transformation critical stress (σ_T = 40 MPa). Based on this difference, we expect that upon loading the martensitic transformation process will preferentially occur in place of plastic deformation at room temperature.

Third, a clear indicative pointing the presence of a martensitic transformation is the low amount of deformation present after the complete unloading (Fig. 3a). While the Cu-Zn-Al foam recovers around 95% of an initial deformation of 3.75%, the pure Cu foam recovers only around 0.2% of a similar strain.

3.2. Dependence of mechanical parameters on the foam relative density

Fig. 5 shows stress-strain curves obtained for foams of different relative densities. It is clear that the linear elastic slope, the transformation stress and the absorbed energy increase as the foam density increases. These different properties can be analyzed in terms of a power-law expression of the type:

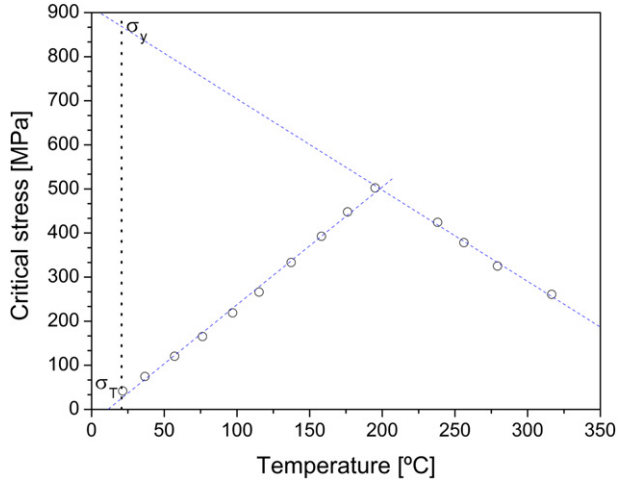

Fig. 4. Critical stress as a function of the test temperature of the bulk material ($\rho/\rho_{bulk} = 1$). There are two different behaviors. At low temperatures, as the temperature increases the critical stress increases. In this range, the critical stress corresponds to the onset of the martensitic transformation. At higher temperatures, the critical stress decreases as the temperature increases, consistent with the typical behavior of materials experiencing plastic deformation.

$$\frac{F}{F_{bulk}} = A\left(\frac{\rho}{\rho_{bulk}}\right)^n \quad (1)$$

where, F and F_{bulk} are the foam and bulk studied property, ρ and ρ_{bulk} are the foam and bulk densities, n is the exponent and A is a constant related to the cell morphology and, in the present case, to the particular transformation properties of the material [25]. The values of the corresponding bulk properties were included in the analysis, therefore $A = 1$ for each case.

Fig. 6a shows the graph of the slope of the linear elastic part of the curve (E) as a function of the foam relative density. In this case, the value of the exponent is $n = 2.31$ and $A = 1$. The theoretical value from dimensional analysis of edge bending deflection gives $n = 2$ and analysis of a tetrakaidecahedral unit cell obtains $A = 0.98$ [26]. The agreement between experimental and theoretical data indicates that SMFs behave like standard metallic foams in the linear elastic regime. A similar analysis can be performed on the stress at the onset of the martensitic transformation. The results are plotted as a function of the foam relative density (Fig. 6b). The analysis based on Eq. (1) for this situation results in $n = 2.15$ and $A = 1$. In the case of the yield stress of an elastic-plastic open-cell foam dimensional arguments give $n = 1.5$ and $A = 0.3$ for Eq. (1). It was found that these values are valid for a wide variety of non-transforming foams and for relative densities up to 0.3 [26]. The

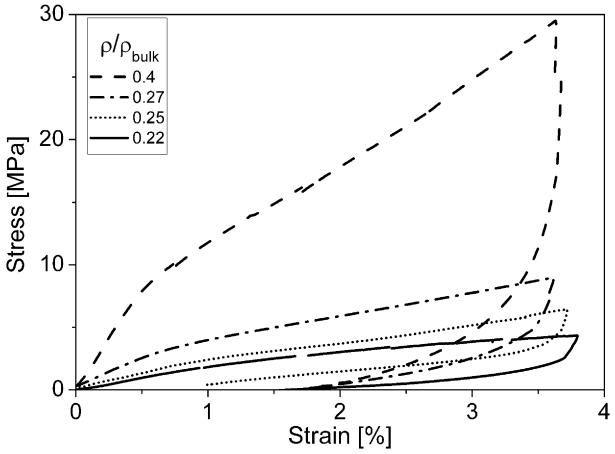

Fig. 5. Stress-strain curves corresponding to compression tests performed on pseudoelastic Cu-Zn-Al foams of different relative densities.

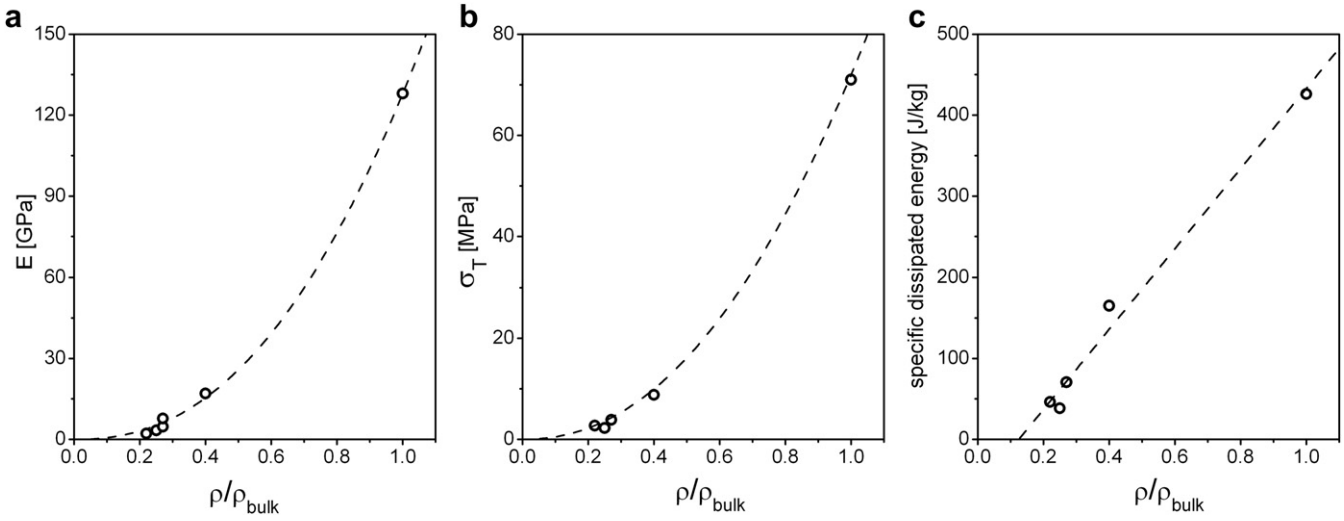

Fig. 6. (a) Slope of the linear elastic part of compression stress-strain curves as a function of the material relative density. (b) Transformation stress measured in compression tests as a function of the material relative density. (c) The specific dissipated energy per cycle as a function of the material relative density. The dotted line represents in the three graphs a least-square power-law fit of the experimental data.

yield stress of standard foams is reached when the struts begin to collapse plastically. Although the shape of stress-strain curves is similar, it has already been explained that in the present case the yield point corresponds to the start of the martensitic transformation and not to the unrecoverable plastic collapse of cells. For this reason, not only the dimensional analysis has to be taken into consideration to assess the variation of the transformation stress with relative density.

Once the stress-induced transformation starts, the stress must be increased in order to further proceed with it. There is no flat transformation plateau in stress-strain curves (Fig. 5), as it would be the case with Cu-Zn-Al single-crystals. The slope observed during the martensitic transformation regime on loading is related to the effect of the local stress and the polycrystalline nature of the foam material. As crystals are randomly oriented, the resolved stress is different for each grain. In addition, stress concentrations occur near the voids, triggering an earlier transformation in those places. It will then be necessary to increase the stress in order to first, to reach the necessary resolved transformation stress in grains not favorably oriented and second to advance the transformation to parts of the material away from pores. Moreover, grain boundaries act as obstacles for the martensitic plates growth. This fact generates additional local stress concentrations which increase the measured macroscopic stress.

Fig. 6c shows that the specific dissipated/absorbed energy by the foam per mechanical cycle, i.e. the area enclosed by the transformation/retransformation cycle normalized by the foam density, grows linearly with relative density. In other words the corresponding exponent Eq. (1) is $n = 2$. This particular behavior is, *a priori*, not obvious. The retained energy in the material is related to the formation of interphases and the friction associated to the movement of the interphases through the material. The dissipated energy is mainly constituted by heat and some acoustic emission associated to the transformation process. In practice, dissipated and retained energies would strongly depend on the retransformation stress level and the relative slope between the transformation and retransformation parts of the curve.

The results presented in Fig. 6 show that the main foam mechanical parameters, i.e. linear elastic behavior, transformation stress and absorbed/dissipated energy per cycle, respond to a similar power-law dependence respect to the foam relative density. Knowing these power-law variations allows designing foams to perform damping in particular processes, simply by choosing their relative density.

Fig. 7 presents the plot of the percentage of recovered strain as a function of the maximum attained strain for foams of different densities. This is a measurement of the effective pseudoelastic capacity of each material. In all cases, the samples recover around 90% of an applied deformation below 4%. At strain levels around 5% the shape recovery level decreases. However, even in this case all samples recover more than the 80% of the imposed deformation.

3.3. Damping capacity

To evaluate the possible utilization of the foams under study as components in damping applications, it is important to know how the cycle frequency as well as the vibration amplitude affects the damping capacity of the material. When pseudoelastic foams are solicited in constrained compression, the deformation cycle is composed by an elastic deformation part and a region where the material deforms transforming to martensite. When the strain amplitude grows, the deformation associated with the martensitic transformation increases as compared to the elastic one, thus increasing the damping capacity.

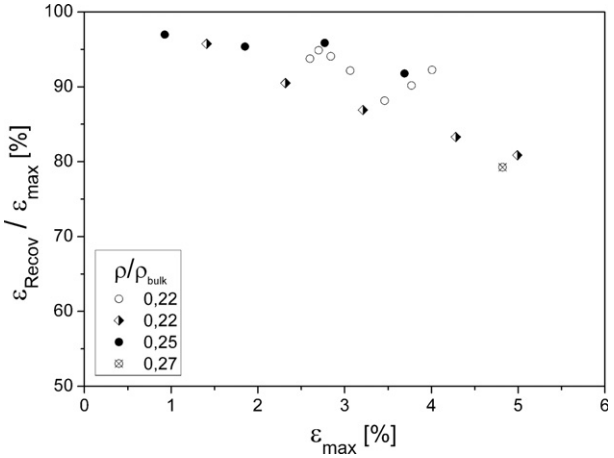

Fig. 7. Amount of recovered strain as a function of the maximum attained strain for foams of different densities.

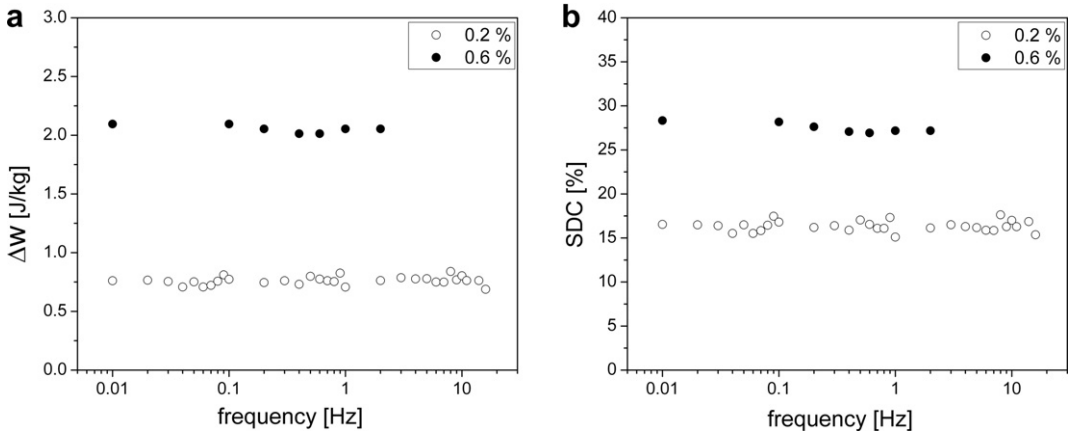

Fig. 8. (a) Specific dissipated energy as a function of the frequency for cyclic tests performed at two different strain amplitudes. (b) Specific damping capacity as a function of the frequency for cyclic tests performed at two different strain amplitudes.

Two equivalent parameters are frequently used in the literature to characterize the damping capacity of materials or devices: the specific damping capacity (SDC), a dimensionless parameter defined as the ratio between the dissipated energy (ΔW) and the maximum strain work in a pseudoelastic cycle (W) [27], Eq. (2), and the loss factor η, as employed by Piedboeuf et al. [28], Eq. (3).

$$\mathrm{SDC} = \frac{\Delta W}{W} \tag{2}$$

$$\eta = \frac{1}{2\pi}\frac{2\Delta W}{U}, \text{ where } U = W - \frac{1}{2}\Delta W \tag{3}$$

In this work the material damping capacity is presented by employing the specific damping capacity (SDC). Next subsections present both the frequency dependence and the amplitude dependence of this parameter.

3.3.1. Frequency dependence of SDC

Experiments were performed on foam samples **f** (Table 1) in order to study the effect of varying the cycling frequency on the SDC. The samples were pre-strained in compression up to 2.1%. From that point, they were cycled at different frequencies in the range of 0.01–20 Hz, and at two different strain ranges, ±0.1% and ±0.3%, i.e. 0.2% and 0.6% strain amplitude, respectively. Fig. 8a shows the specific dissipated energy as a function of the cycling frequency while Fig. 8b shows the specific damping capacity, again as a function of the cycling frequency. SDC values vary from 17% to 27% for strain levels of 0.2% and 0.6%, respectively. The figures show that both, the specific dissipated energy and SDC, are independent of the cycling frequency in the studied frequency and strain ranges. In general, at low frequency levels, effects on the SDC in shape memory alloys are associated to the dissipation of heat generated by the samples. For example, this is a well known effect in Ni-Ti where a combination of high transformation enthalpy and relatively low thermal conduction results in a strong frequency dependent behavior [27,29]. In the case of Cu-Zn-Al foams, the heat is efficiently removed by the material high thermal conduction, enhanced by the particular open morphology of the foam itself. For these reasons, there is no noticeably effect of the cycling frequency in the current test conditions.

3.3.2. Amplitude dependence of SDC

We have also investigated the variation of SDC with the applied strain at a fixed cycling frequency of 1 Hz. Samples of foam type **f** (Table 1) were first pre-strained by 2.1% in compression inducing a partial martensitic transformation. From this point, cyclic deformation was applied. Fig. 9 shows the results corresponding to strain

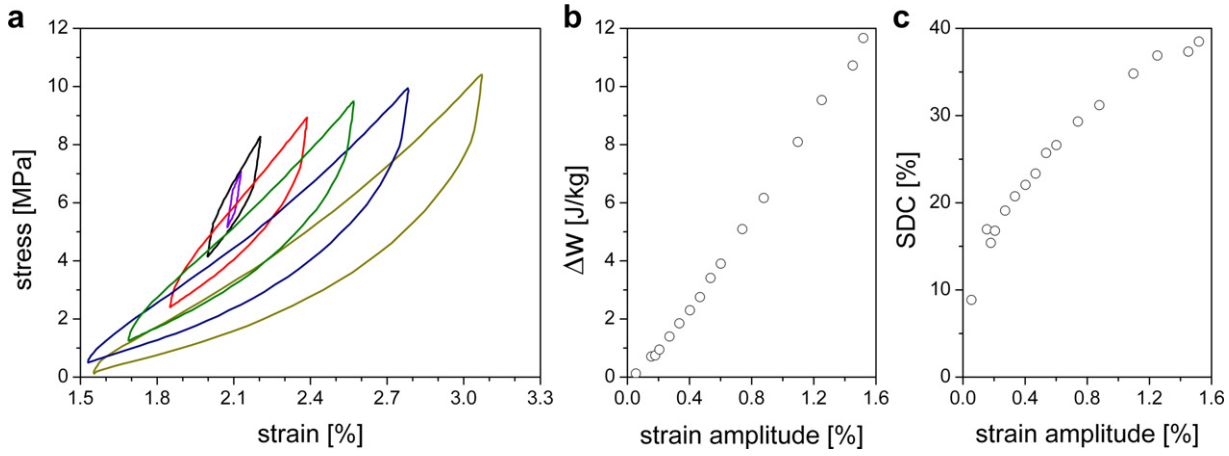

Fig. 9. (a) Stress-strain loops measured at different strain amplitudes for a foam sample type **f** (see Table 1). The cycling frequency was 1 Hz in all cases. (b) Variation of the specific dissipated energy with the strain amplitude. (c) Variation of the specific damping capacity with the strain amplitude.

amplitude variations between 0.1% and 1.5% in a single sample. Fig. 9a presents examples of stress-strain loops. For each strain level, 100 cycles were performed and the last cycle is shown in the figure. Experiments were performed in order, the strain amplitude was incremented from the smallest to the highest value. The slope corresponding to the martensite formation part of the first, smaller cycles, is steeper compared with the last cycles. In addition, there is a certain relaxation in transformation stress values. The last cycles occur at lower transformation stresses than the low amplitude ones. This behavior reflects the fact that cycling progressively "trains" the material by generating nuclei of retained martensite which facilitate subsequent transformations. Fig. 9b and c show the variation of the specific dissipated energy and SDC with the strain amplitude, respectively. In the former, the dissipated energy increases almost linearly with the applied strain amplitude. The variation occurs because the material forms a higher amount of martensite as the strain increases. In previous studies it has been shown that the linear variation can be easily rationalized when the transformation/retransformation cycle shape does not change with increasing applied strain [28,30]. The present case, although more complicated because there is no constant stress transformation plateau, preserves the linear dependence indicating a similar overall behavior.

The variation of SDC shown in Fig. 9c indicates that the material is more effective to absorb energy at higher strain intervals, reaching almost 40% SDC at 1.5% strain amplitude.

3.3.3. Constrained cyclic loading behavior

In order to illustrate the possibility of using SMFs for concrete damping applications, we studied their mechanical behavior on constrained compression cycling tests. To illustrate the observed behavior, results are presented for a foam sample with a density of 2350 kg/m^3 corresponding to a relative density of 0.28 and mean pore size of 2 mm (foam type **c**, Table 1). Based on the experiments shown in the previous sections, the foam was first pre-strained at 2.65%, inducing a certain amount of martensite in the sample. The pseudoelastic cyclic experiment was then performed by imposing the strain limits between 1.5% and 3.8%. Fig. 10a shows the mechanical stress-strain behavior of the foam when subjected to 1000 transformation cycles. For the sake of clarity, only the last of every 100 cycles are presented in the figure. Remarkably, the mechanical behavior of the sample remained stable for these repeated operations. The imposed deformation is recovered pseudoelastically with almost no change in the main features of the cycles. Intergranular fracture, observed in similar foams at higher strain levels [24], was not detected in this case except on some isolated regions of the external surface. Fig. 10b presents the variation of the limit stress levels associated to the imposed deformation range. The variations of these minimum and maximum stresses along the cycling operation are relatively small indicating a low material degradation for these operation conditions. The increase on the maximum stress on the cycles resembles a strain-hardening behavior. In the present case it could be due to an increase in the number of obstacles such as pinned martensite plates.

As it was shown in Fig. 7, full loading/unloading cycles for different density foams resulted in some retained deformation because the material does not return to exactly the same state after the external stress is eliminated. However, as it is clear from Fig. 10a, this can be prevented if the material works in a constrained length range avoiding the external stress to vanish. For the situation shown in Fig. 10 the material recovers its macroscopic shape after a complete closed cycle. The experiment demonstrates the possibility of implementing damping devices working between fixed deformations boundaries. This new type of material presents the possibility of working in repeated damping cycles with a minimum structural degradation. This fact constitutes a remarkable difference as compared to Al foams which undergo irrecoverable deformation in damping applications. For Al foams [31] the absorbed energy varies between 0.1 MJ/m^3 and 5 MJ/m^3 up to the densification point. The new material foam presented here absorbs 40 kJ/m^3 per cycle within the deformation limits shown in Fig. 10. Even considering this value is smaller than the corresponding for Al foam, it is important to remember that SMF material is not being brought to densification and that it can work in cyclic operation, allowing its repetitive use in dynamical applications.

3.4. SEM observations

We have performed SEM observations SMF type **c** (Table 1) subjected to 1000 compression cycles in order to identify possible microstructural changes due to mechanical cycling. Example images are shown in Fig. 11. The surface of different pores have an inhomogeneous aspect across the sample, while some pores appear free from surface defects others contain a variety of them like those shown in Fig. 11a and b. The difference occurs due to two main factors. On the one hand, the material grains have different crystallographic orientations and therefore, under the applied stress diverse martensite variants will grow. On the other hand, the particular structure of the foam produces inhomogeneous stress distributions across the material. As a consequence, different grains evidence different amounts surface defects. This situation can be

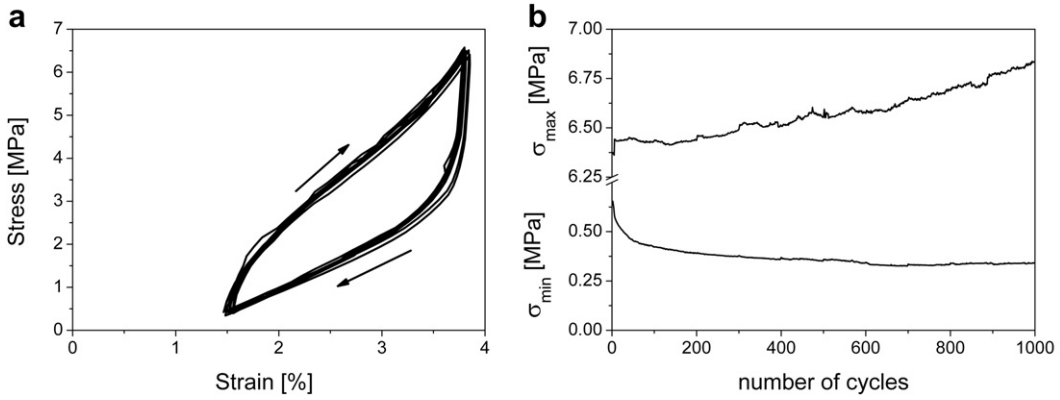

Fig. 10. Results of constrained compression cycling tests on a Cu-Zn-Al foam with 0.28 relative density. The cycles were performed by controlling the strain limits between 1.5% and 3.8%. (a) The last of every hundred cycles for 1000 compression cycles. (b) Variation of the upper and lower stress limits as a function of the number of cycles.

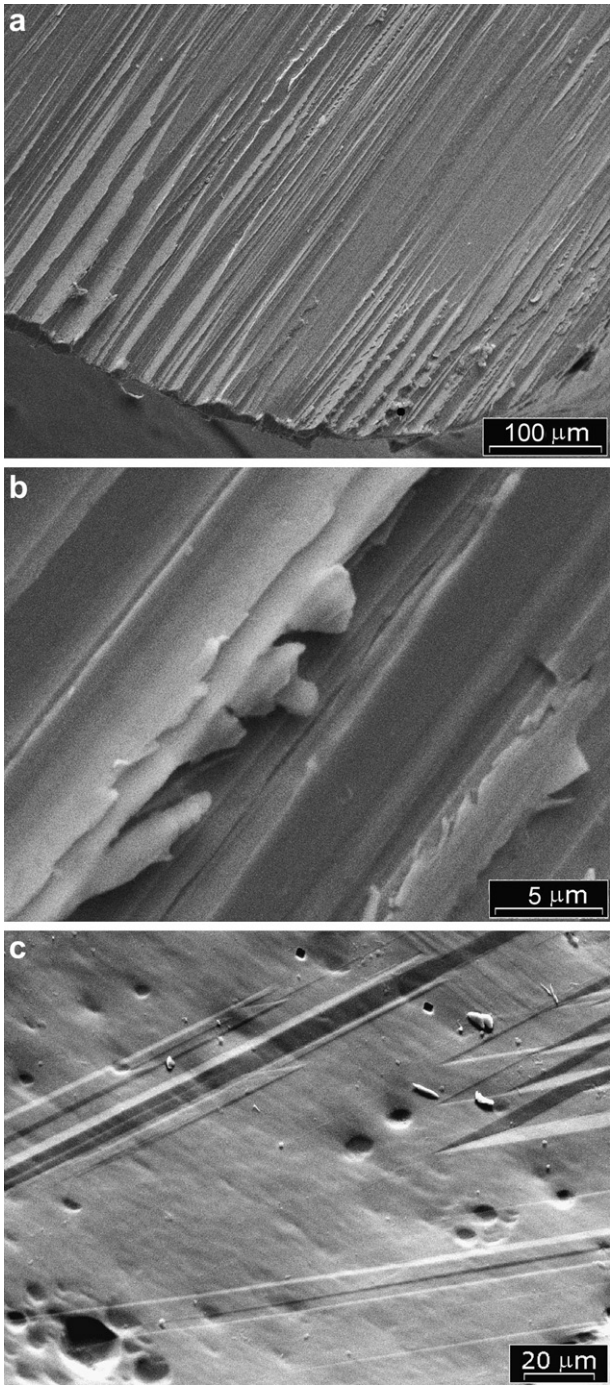

Fig. 11. SEM images of a Cu-Zn-Al foam after 1000 cycles. (a) Grains with different surface features. (b) Detail of the intrusion-extrusion like defects present in the central grain shown in Fig. 11a. (c) Scattered retained martensite plates along the surface.

observed in Fig. 11a. There, at the center of the image there is a grain with a relatively large density of surface defects. Next to this grain, on the lower left-hand side of the image, there is another grain which appears nearly free from defects. This heterogeneous aspect is frequently observed in cycled Cu-Zn-Al polycrystalline samples [32]. Fig. 11b shows a close up image of the lower right side of the deformed grain shown in Fig. 11a. The observed features can be identified as the intrusion-extrusion defects found in fatigued Cu-Zn-Al single-crystals [32,33]. These defects could be a consequence of the gradual accumulation of permanent slip over the whole cyclic experiment. Fig. 11c shows the presence of some scattered retained martensite plates. This is also a feature frequently observed in these cycled samples. It indicates the presence of residual deformation, and occurs preferentially when the M_s temperature of the alloy is close to room temperature. These residual plates can act as nucleation sites for the stress-induced martensite, leading to the relaxation phenomenon observed, for example, in Fig. 9a. However, the deformation associated to the presence of these residual plates is recoverable because they disappear when the sample is heat up to a point above the austenite finish temperature (A_f).

4. Concluding remarks

1) Cu-Zn-Al metallic foams can undergo large deformations by producing a martensitic phase transformation. They pseudoelastically recover a large amount of this deformation upon unloading. The material dissipates energy in the process. The studied foams do not need a thermomechanical treatment of any kind to achieve the reported properties.
2) Relevant properties of the material present a power-law variation as a function of the relative density. In particular, this variation was confirmed for the specific energy absorbed in pseudoelastic cycles. This information is useful for designing damping devices and establishes the foam density as a governing parameter also for transformation properties.
3) The specific damping capacity of the material remains independent of the cycling frequency in the four decades range between 0.01 Hz and 20 Hz at fixed strain amplitudes between 0.1% and 0.6%. This is a useful frequency range when considering structural damping applications. In addition, we have found that the specific damping capacity increases with the increment of the applied strain amplitude, reaching around 40% at a strain amplitude of 1.6%.
4) The material shows remarkable mechanical stability in the studied range of constrained cyclic compression tests.

Acknowledgments

The authors gratefully acknowledge the financial support of ANPCyT (Argentina) and CONICET (Argentina) and DIUC (grant 209.098.001–1.0).

References

[1] Van Humbeeck J. Damping capacity of thermoelastic martensite in shape memory alloys. J Alloys Compd 2003;355:58–64.
[2] Banhart J. Manufacture, characterisation and application of cellular metals and metal foams. Progr Mater Sci 2001;46:559–632.
[3] Qiao P, Yang M, Bobaru F. Impact mechanics and high-energy absorbing materials: review. J Aerospace Eng 2008;21:235–48.
[4] Bansiddhi A, Sargeant TD, Stupp SI, Dunand DC. Porous NiTi for bone implants: a review. Acta Biomater 2008;4:773–82.
[5] Saburi T. Ti-Ni shape memory alloys. In: Otsuka K, Wayman CM, editors. Shape memory materials. Cambridge: Cambridge Univ. Press; 1998. p. 49–96.
[6] Yuan B, Chung CY, Zhu M. Microstructure and martensitic transformation behavior of porous NiTi shape memory alloy prepared by hot isostatic pressing processing. Mater Sci Eng A 2004;382:181–7.
[7] Bansiddhi A, Dunand DC. Shape-memory NiTi foams produced by replication of NaCl space-holders. Acta Biomater 2008;4:1996–2007.
[8] Xiong JY, Li YC, Wang XJ, Hodgson PD, Wen CE. Titanium–nickel shape memory alloy foams for bone tissue engineering. J Mech Behav Biomed Mater 2008;1:269–73.
[9] Greiner C, Oppenheimer SM, Dunand DC. High strength, low stiffness, porous NiTi with superelastic properties. Acta Biomater 2005;1:705–16.
[10] Zhao Y, Taya M, Kang Y, Kawasaki A. Compression behavior of porous NiTi shape memory alloy. Acta Mater 2005;53:337–43.
[11] Itin VI, Gyunter VE, Shabalovskaya SA, Sachdeva RLC. Mechanical properties and shape memory of porous Nitinol. Mater Charact 1994;32:179–87.

[12] Li BY, Rong LJ, Li YY. Stress-strain behavior of porous Ni-Ti shape memory intermetallics synthesized from powder sintering. Intermetallics 2000;8: 643–6.
[13] Locci AM, Orrù R, Cao G, Munira ZA. Field-activated pressure-assisted synthesis of NiTi. Intermetallics 2003;11:555–71.
[14] Biswas A. Porous NiTi by thermal explosion mode of SHS: processing, mechanism and generation of single phase microstructure. Acta Mater 2005; 53:1415–25.
[15] Zanotti C, Giuliani P, Terrosu A, Gennari S, Maglia F. Porous Ni-Ti ignition and combustion synthesis. Intermetallics 2007;15:404–12.
[16] Zhang XP, Liu HY, Yuan B, Zhang YP. Superelasticity decay of porous NiTi shape memory alloys under cyclic strain-controlled fatigue conditions. Mater Sci Eng A 2008;481-482:170–3.
[17] Li YH, Rao GB, Rong LJ, Li YY, Ke W. Effect of pores on corrosion characteristics of porous NiTi alloy in simulated body fluid. Mater Sci Eng A 2003;363:356–9.
[18] Sadrnezhaad SK, Hosseini SA. Fabrication of porous NiTi-shape memory alloy objects by partially hydrided titanium powder for biomedical applications. Mater Design 2009;30:4483–7.
[19] Hyun SK, Nakajima H. Fabrication of porous iron by unidirectional solidification in nitrogen atmosphere. Mater Trans 2002;43:526–31.
[20] Wang Q, Han F, Wu J, Hao G. Damping behavior of porous CuAlMn shape memory alloy. Mater Lett 2007;61:2598–600.
[21] Castrodeza EM, Mapelli C, Vedani M, Arnaboldi S, Bassani P, Tuissi A. Processing of shape memory CuZnAl open-cell foam by molten metal infiltration. J Mater Eng Perf 2009;18:484–9.
[22] Tadaki T. Cu-based shape memory alloys. In: Otsuka K, Wayman CM, editors. Shape memory materials. Cambridge: Cambridge Univ. Press; 1998. p. 97–116.
[23] Castrodeza EM, Mapelli C. Processing of brass open-cell foam by silica-gel beads replication. J Mater Process Tech 2009;209:4958–62.
[24] Bertolino G, Arneodo Larochette P, Castrodeza EM, Mapelli C, Baruj A, Troiani HE. Mechanical properties of martensitic Cu-Zn-Al foams in the pseudoelastic regime. Mater Lett 2010;64:1448–50.
[25] Gibson LJ. Mechanical behavior of metallic foams. Annu Rev Mater Sci 2000; 30:191–227.
[26] Gibson LJ, Ashby MF. Cellular solids, structure and properties. 2nd ed. Cambridge: Cambridge University Press; 1997.
[27] Heller L, Sittner P, Pilch J, Landa M. Factors controlling superelastic damping capacity of SMAs. J Mater Eng Perf 2009;18:603–11.
[28] Piedboeuf MC, Gauvin R. Damping behaviour of shape memory alloys: strain amplitude, frequency and temperature effects. J Sound Vib 1998;214: 885–901.
[29] Soul H, Isalgue A, Yawny A, Torra V, Lovey FC. Pseudoelastic fatigue of NiTi wires: frequency and size effects on damping capacity. Smart Mater Struct 2010;19. 085006 (7 pp).
[30] Tobushi H, Lin PH, Tanaka K, Makita M, Ikai A. Deformation behavior of Ni-Ti superelastic alloy subjected to strain variations. In: Proc first int conf shape mem superelastic tech, California: SMST; 1994. p. 389–394.
[31] Olurin OB, Fleck NA, Ashby MF. Deformation and fracture of aluminium foams. Mater Sci Eng A 2000;291:136–46.
[32] Sade M, Rapacioli R, Ahlers M. Fatigue in Cu-An-Al single crystals. Acta Metall 1985;33:487–97.
[33] Damiani C, Sade M. Composition dependence of surface and bulk defects generated in Cu-Zn-Al single crystals after pseudoelastic cycling. Mater Sci Eng A 1999;273–275:616–21.